Investigation of the impact of the short fiber reinforcements on the thermal and mechanical properties of polymer-based composites manufactured by material extrusion

Mohammad Ahmadifar[1,2] · Mohammadali Shirinbayan[2] · Khaled Benfriha[1]

Abstract

In the recent years, additive manufacturing (AM) has been widely expanded for manufacturing the polymer and polymer-based composite parts. The main drawback of the material extrusion additive manufactured parts is the weaker mechanical properties in comparison to the manufactured parts by the conventional methods. The stated weak mechanical properties are due to the weak adhesion between the deposited layers. The poor adhesion between the deposited layers in material extrusion additive manufacturing process is due to the fact that the previous deposited filament (n-1) is already cooled and solidified. To ensure the appropriate adhesion between the two adjacent filaments, the temperature of the first deposited layer (n-1) has to be high enough to obtain a suitable adhesion to the subsequent layer (n) but in an optimum range to avoid the lack of the dimensional accuracy. Therefore, a precise and local measurement of the temperature on the scale of the diameter of the filaments is necessary. In this study, four important process parameters (liquefier temperature, layer height, print speed, and bed platform temperature) were selected to study their effects on the rheological behavior and temperature evolution of the PA6 and CF-PA6 materials during material extrusion process. Then, the impact of the short/chopped reinforcement on the thermal and mechanical properties of the material extrusion additive manufacturing processed polymer-based composites were studied by comparing the obtained results from PA6 and CF-PA6 parts. In one experiment, it was observed that increasing the liquefier temperature from 220 to 240 °C increased the tensile strength and crystallinity percentage of the manufactured PA6 and CF-PA6 specimens. It was determined that the crystallinity percentages of PA6 and CF-PA6 specimens increased from 12.51 to 14.40% and from 19.97 to 20.51%, respectively. One of the existence effects of carbon fibers is highlighted in the higher crystallinity values of the CF-PA6 specimens comparing PA6 specimens. Finally, a time–temperature-transformation diagram was plotted to determine the processability condition of the utilized materials. It can be helpful for the designers and researchers to find out the optimal material extrusion additive manufacturing process parameters condition for the utilized raw materials.

Keywords Material extrusion · Process parameters · Temperature · Mechanical properties · Processability

1 Introduction

Additive manufacturing (AM) is introduced to produce objects from digital 3D models, typically layer by layer, as opposed to subtractive manufacturing [1, 2]. In AM, computer-aided design (CAD) files of objects are converted into physical models utilizing different manufacturing processes [3–5]. AM, also known as 3D printing, includes the different methods such as: laminated object manufacturing (LOM) is relying on plastic lamination [6], stereolithography apparatus (SLA) relies on photo polymerization [7], selective laser sintering (SLS) relies on fusion of the powders [8], and fused filament fabrication (FFF) is relying on the melting

✉ Mohammad Ahmadifar
mohammad.ahmadifar@ensam.eu

Mohammadali Shirinbayan
mohammadali.shirinbayan@ensam.eu

Khaled Benfriha
khaled.benfriha@ensam.eu

[1] Arts Et Metiers Institute of Technology, CNAM, LCPI, HESAM University, 75013 Paris, France

[2] Arts Et Metiers Institute of Technology, CNAM, PIMM, HESAM University, 75013 Paris, France

of polymer/composite filaments [9, 10]. FFF and SLS are the most widely used AM methods for polymer composites. However, FFF has traditionally been deemed to be the most effective process.

Comparatively speaking, FFF process provides the following advantages: Multiple materials can be deposited simultaneously, requiring little energy input, having readily available raw materials, being less likely to degrade, being more affordable, not requiring chemical modifications after the manufacturing process on the products, and being able to offer a wide range of printers at various prices [11–20]. Various thermoplastic polymer/composite filaments, such as acrylonitrile butadiene styrene (ABS), polylactic acid (PLA), polyimide (PA), etc., are applied to feed FFF printers. The liquefier temperature is set above the filament melting point. Consequently, the filament will be softened and melted inside the liquefier. Then, the molten material will be pushed by the still-solid upstream filament through the nozzle and will be deposited on the platform bed. For each layer of the object, the extruded polymer is laid down as the nozzle moves, starting with the perimeters and moving towards the filling [21, 22].

Several studies are conducted on the manufacturing and development of filaments utilized in the FFF process. Zander et al. [23] conducted experiments to fabricate polyethylene terephthalate filament and introduced the recycled PET as filament. Printed specimens as well as filaments processed with different conditions were evaluated for their thermal and mechanical properties. Utilization of the recycled filaments made from HDPE and poly (lactic acid) for FFF process has been reported [24, 25].

There are several advantages concerning the short fiber reinforced polymers (SFRP), including improvements in mechanical properties, facilitation in fabrication, and their affordable price [26–28]. Numerous studies have been conducted on the mechanical behaviors and dimensional stability of the FFF processed parts. The effects of printing parameters, including extrusion rate and cooling, on dimensional accuracy and bonding strength were discussed by Costa et al. [29]. Utilizing the FFF feedstock of ABS reinforced with carbon nanotubes, Shofner et al. [30] reported an improvement in tensile strength of 40% and modulus of 60% when neat ABS was reinforced by 10% wt carbon nanotubes. Ahmadifar et al. [31] investigated the effect of liquefier temperature, layer height, bed temperature, and print speed as the four important process parameters on the thermal and mechanical behaviors of the FFF-printed chopped carbon fiber reinforced PA6 composite specimens. This was accomplished by measuring the in-situ temperature and thus studying the rheological behavior of the chopped carbon fiber reinforced PA6 during the FFF process. B. Brenken et al. [32] tried to predict final deformed shapes and residual stresses of printed 50 wt.% carbon fiber reinforced PPS material caused by the printing process. Using FFF manufacturing, Ankit Gupta et al. [33] investigated the mechanical properties of the short carbon fiber (SCF) reinforced polycarbonate composite. In this experiment, the specimens were printed with the different carbon fiber volume fractions (3%, 5%, 7.5%, and 10%) and different print speeds (25, 50, and 75 mm/s). Two variables were found to heavily influence mechanical properties of printed specimens, which was volume fractions of short carbon fibers and printing speed. The effect of layer thickness and liquefier temperatures on the tensile strength of carbon fiber reinforced PLA have been investigated by Durga et al. [34]. Their study considered varying liquefier temperatures (205, 215, and 225 °C) as well as layer thicknesses (0.1, 0.2, and 0.3 mm). Accordingly, the manufactured sample with the smallest selected layer thickness and the highest selected liquefier temperature demonstrated the greatest tensile strength. Ning et al. [35] investigated the FFF processing of carbon fiber (CF) reinforced ABS parts by varying the reinforcement lengths and contents. Incorporating 5% of CF increased the tensile and flexure strength by 22.5% and 11.8%, respectively. Furthermore, the samples with CF average length of 150 μm exhibited a greater modulus and strength than the samples with CF average length of 100 μm. According to Zhong et al. [36], ABS composite containing glass fiber reinforcements had development in the tensile strength but diminution in the filament flexibility.

Nevertheless, more research and investigation are required to be conducted regarding the mechanical characteristics of the FFF-processed short fiber reinforced polymer parts and their dimensional accuracy. During this research, an attempt was made to study and understand the effect of chopped carbon fibers as utilized short reinforcements on the temperature evolution and rheological behaviors of the material during FFF process and consequently on the dimensional stability and mechanical behavior of the fabricated specimens. In order to analyze the processability of the utilized raw materials, the time–temperature-transformation diagram was plotted to identify the optimal parameters for the additive manufacturing process.

2 Material description, 3D printer device, and characterization methods

2.1 Material and sample preparation

The purpose of this research was studying the role of the short reinforcement fibers on the thermal and mechanical behavior of FFF-fabricated specimens. Thus, a polymer filament and a polymer composite filament were utilized to be able to investigate the effect of the short reinforcement fibers. Indeed, the matrix component of the composite filament

was the same material that had been selected as the utilized polymer filament. The selected polymer and composite filaments for this study were made of PA6 and chopped carbon fiber reinforced PA6 (CF-PA6), respectively. The utilized PA6 and CF-PA6 filaments are commonly known as Nylon White and Onyx, respectively, developed by Markforged®. Based on the conducted pyrolysis analysis, the composite material (CF-PA6) contained 6.5% chopped carbon fibers with the size range of 10–312 µm. The density of the Nylon White and Onyx filaments were 1.1 g/cm^3 and 1.2 g/cm^3, respectively. Moreover, the diameter of these filaments was 1.75 mm (±0.01 mm). A set of PA6 and CF-PA6 manufactured specimens were fabricated for the purpose of examining the effects of the four selected process parameters (Sect. 2.2) on the thermal and mechanical properties of the printed specimens.

According to the investigation of the role of the short reinforcements on the thermal and mechanical behavior of FFF-fabricated specimens, the sample geometry was designed as shown in Fig. 1a. In this regard, specimens were printed following the parameters shown in Table 1. Then, the effect of the chopped carbon fibers was examined in the fabricated specimens under the selected process parameters. Consequently, several tests and characterizations were carried out. Therefore, the height of this single wall was determined to be as high as necessary to allow the extraction of specimens necessary for characterizations (such as tensile test and DSC). The locations of the relevant samples are specified in Fig. 1b. It is remarked that a visual inspection was conducted on the prepared tensile test samples to ensure that macro holes were not present. Moreover, the in situ monitoring of the temperature profile evolution was performed during the construction of the single-wall sample (Fig. 1).

Table 1 The selected FFF process parameters

Condition no	$T_{Liquefier}$ (°C)	T_{Bed} (°C)	V (mm/s)	Layer height (mm)
No. 1	220			
	230	25 ± 0.5	15	0.1
	240			
No. 2			13	
	240	25 ± 0.5	15	0.1
			17	
No. 3				0.1
	240	25 ± 0.5	15	0.2
				0.3
No. 4		25 ± 0.5	15	
	240	45 ± 1		0.1
		62 ± 1		
		79 ± 1		

2.2 Process parameter classification

In regard to the FFF process, different 3D printers offer a wide selection of process parameters. By the additive manufacturing process, the process parameters have a crucial role in the bonding of the consecutive printed layers and consequently the mechanical properties of the manufactured parts. In this study, the effects of four main FFF parameters were investigated: the temperature of liquefier ($T_{Liquefier}$), bed platform temperature (T_{Bed}), print speed (V), and layer height (h). The selected printing conditions for specimens are identified as Nos. 1, 2, 3, and 4 in Table 1. As for the study of each parameter individually, it was tried to keep the other parameters in the stated constant values (Table 1).

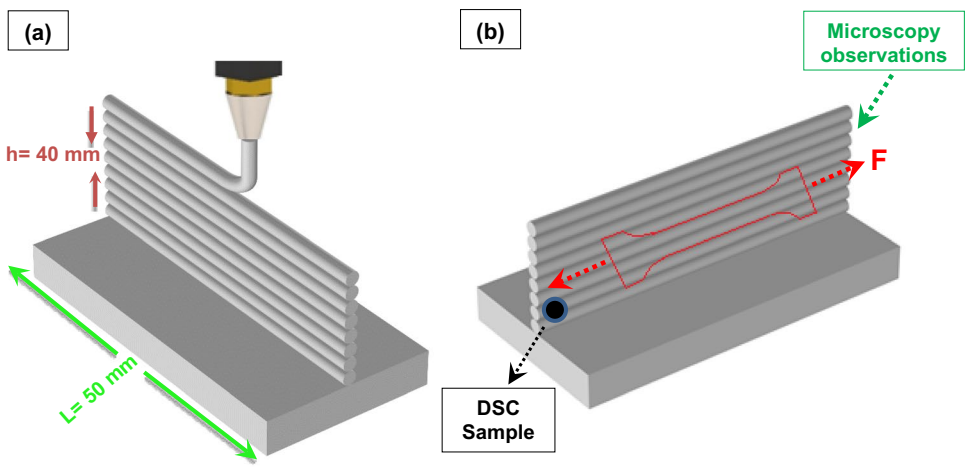

Fig. 1 Schematic of the fabricated specimen (the single-wall layer specimen)

3 Materials and methods

3.1 Microscopic observation

An optical microscope (OLYMPUS BH2) has been utilized to obtain a qualitative assessment of the printed specimens at different process parameters with 100 to 500 µm magnifications. A scanning electron microscope (HITACHI 4800 SEM—high resolution (better than 1 nm)) also has been used. The microscopy observations were used to evaluate the quality and dimensional accuracy of the final manufactured specimens. Furthermore, microscopy observation was conducted to analyze the distribution and the size range of the chopped carbon fibers throughout the CF-PA6 filament.

3.2 DSC

Utilizing differential scanning calorimetric (DSC), the temperature of the samples was compared with the reference sample while they were being heated. DSC enabled the determination of the crystallization and glass transition temperatures, as well as the heat capacity of the raw materials (PA6 and CF-PA6), and the fabricated specimens under the selected processing conditions. In this regard, DSC Q1000 was utilized. Analyses of the raw materials (PA 6 and CF-PA 6) were conducted at three ramp temperatures ranging from − 70 to 220 °C. Therefore, the first ramp erased the thermal history of the sample. Consequently, the results were obtained in controlled conditions. As for the result, the below curves (Fig. 2 a and b) were obtained. The obtained glass transition, melting and crystallization temperatures were identified in Fig. 2. Moreover, the DSC analysis of the printed specimens was performed in two ramps (heating and cooling) ranging from 20 to 220 °C. Significant consideration was given to the crystallinity zone taken from the DSC curves. In this zone, diffusion which ultimately leads to adhesion and bonding of the layers occurs, which also impacts the dimensional accuracy of the printed samples, directly. The rate of the heating and cooling cycles was 10 °C/min.

3.3 DMTA measurement

Utilizing the DMA Q800 instrument from TA Company, thermo-mechanical analysis (DMTA) flexural tests have been performed on the printed specimens to determine their major transition temperatures and their viscoelastic properties. The flexural test was conducted at the following condition: temperature range varying from 10 to 80 °C, temperature rate of 2 °C/min, and the frequencies of 1, 2, 5, 10, and 30 Hz.

3.4 Rheological characterization

The rheological characterization of the CF-PA6 and PA6 filaments was carried out by means of Rheometer MCR502 from Anton paar. The experimental tests were conducted with plate-plate measuring system under the protected atmosphere by nitrogen flow. The filaments of the stated raw materials were cut into several pieces to cover the utilized parallel plate configuration surface of the rheometer Machine. The test was conducted in controlled-strain condition of 0.2% and frequency ranging from 0.01 to 100 rad/s. As the result of this experiment, the viscoelastic behaviors of the materials in both Newtonian and non-Newtonian zones at the different applied printing temperature values of 210, 220, 230, and 240 °C were determined.

3.5 Quasi-static tensile test

Tensile test specimens were obtained from the single-wall printed layers (Fig. 1a). So, the deposited layers in the tensile test specimens were unidirectional and the related angle

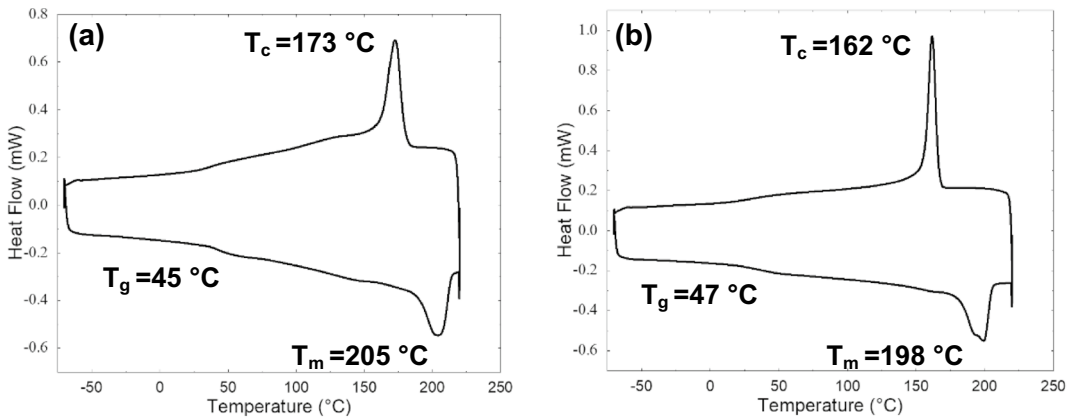

Fig. 2 DSC characterization of **a** PA6 filament and **b** short carbon fiber-reinforced PA6 (CF-PA6) filament

was 0 °C. Figure 3 depicts the dimension of the tensile test specimens used for mechanical testing as determined by ISO 527–2. The tensile test was conducted on a minimum of three specimens related to the each considered fabrication condition. Using the INSTRON 4301 machine, tensile tests were carried out under the displacement rate of 5 mm/min.

3.6 *In situ* evaluating of the temperature concerning the deposited layers during FFF

An Optris PI450 infrared camera was utilized to study the effects of process parameters on the temperature evolution of polymers and polymer-based composites during the FFF process. According to the specifications of this camera, the related optical resolution, wavelength range, frame rate, accuracy values, and frequency were 382 × 288 pixels, 8–14 µm, 80 Hz, ± 2%, and 32 Hz, respectively. In order to achieve a uniform plain field of view (FOV) of all consecutive printed and deposited layers, the stated infrared camera was applied with the determined and specific distance from the extruder (Fig. 4). The temperature profile was recorded for the first deposited layer in the sequence of the subsequent deposits at a predetermined location starting with the first deposit.

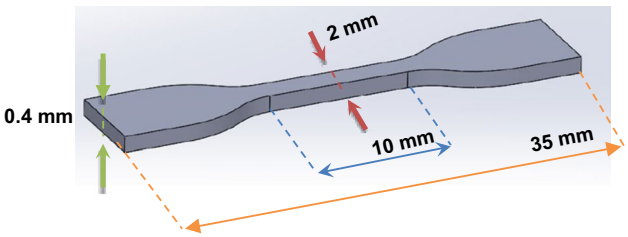

Fig. 3 The geometry of the used tensile test specimen

4 Results and discussions

4.1 Characterization of the used filament (raw material)

4.1.1 Microstructure analysis

A piece of the CF-PA6 filament was observed under the optical microscope (Fig. 5a). According to the obtained observation, the chopped carbon fibers were almost unidirectional, and they were oriented along the filament length. These observations can be attributed to the extrusion manufacturing process, in which the filaments are manufactured. Also, the size range of the chopped carbon fibers was investigated after the pyrolysis of the CF-PA6 filament (Fig. 5b). The pyrolysis process was carried out at 500 °C for 5 h. Carbon fibers were found to range in size from 10 to 312 µm, based on the performed observations. The diameter of the both PA6 and CF-PA6 filaments were about 1.75 mm (± 0.01 mm).

4.1.2 Thermo-mechanical behavior characterization

The thermo-mechanical behavior characterization of CF-PA6 filament was conducted using the DMTA test. As for the result, the below curve (Fig. 6) was obtained. Main transition temperatures due to molecular mobility as

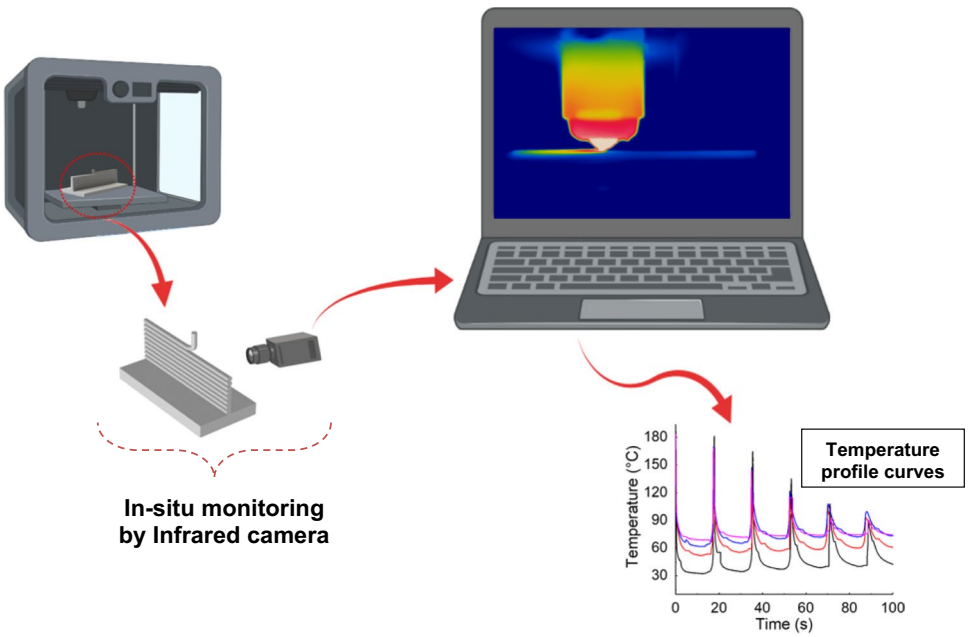

Fig. 4 In situ monitoring of temperature evolution during FFF process

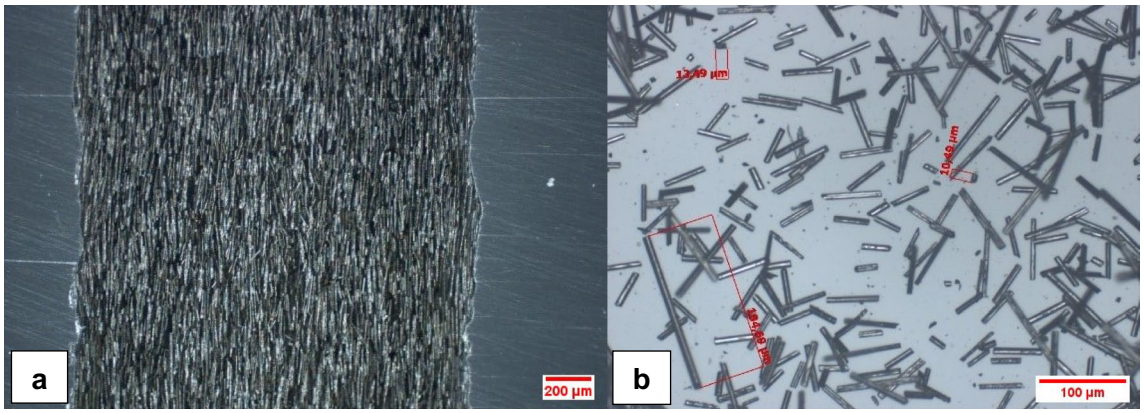

Fig. 5 Microstructure observation: **a** investigation of the carbon fibers in a piece of the CF-PA6 filament; **b** investigation of the size range of the carbon fibers after pyrolysis [31]

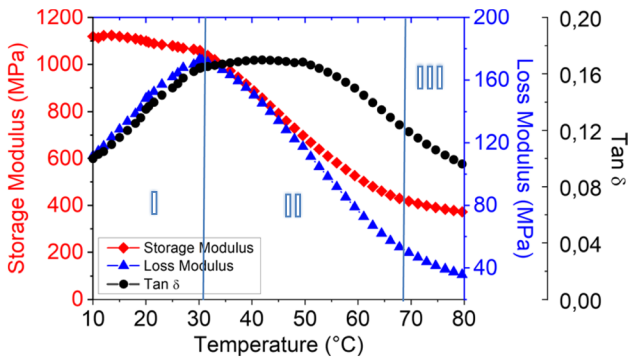

Fig. 6 DMTA test result: Evolution of the storage, loss moduli, and loss factor versus temperature

a function of the temperature have been measured using the DMTA test. As it can be noticed, CF-PA6 presented a glass transition of nearly 47 °C.

The elastic or viscous response of CF-PA6 can be measured as a function of temperature using DMTA; it is possible to understand the true internal damping of the system. One can suppose that CF-PA6 has stable rigidly at the ambient temperature while the storage modulus continues to decrease slowly until 80 °C due to the increase of macromolecular chain mobility.

However, since the thermomechanical behavior of the polymer determines the diverse transitions and change of physical state of polymer, DMTA test is implemented using the alternating bending configuration (with the frequency of 1 Hz). Figure 6 illustrated the three physical states: glassy state (I), glass transition zone (II), and rubbery state (III). Based on Fig. 6, the material exhibits a glassy state up to ~ 30 °C. In glassy state, E' is relatively high (~ 1100 MPa). The second zone (30 °C < T < 65 °C) correspond to glass transition zone. E' decreases drastically from ~ 1100 MPa to a value lower than 400 MPa. The rubbery state of the material is then the zone of temperature higher than 65 °C. Presumably, the value of E' is low and the sample is relatively soft.

4.2 Effect of process parameters

4.2.1 Influence of liquefier temperature

The effect of the liquefier temperature as the most important process parameter of the manufactured samples made of CF-PA6 and PA6 was investigated. For this purpose, three different liquefier temperature values of 220, 230, and 240 °C were selected for comparing their effects on the manufactured samples. The obtained DSC curves illustrated the impact of liquefier temperature on the crystallization degree and the related heat flow values of the crystallinity (Fig. 7). The calculated crystallization degree of the manufactured samples made of CF-PA6 and PA6 concerning the selected liquefier temperature values are tabulated in Table 2. It is observed that the increase of the liquefier temperature affected the crystallinity temperature (T_c) and the melting temperature (T_m) of the manufactured specimens. Generally, the increase of the liquefier temperature increased the T_c and T_m, while its effect was more highlighted in increase of the melting point of the PA6 and CF-PA6 specimens.

Figure 8 illustrates the tensile behaviors of the PA6 specimens which were manufactured under the considered and stated liquefier temperature values. The maximum tensile strength of the printed specimens under the liquefier temperature of 230 °C and 240 °C were 55.48 ± 0.78 MPa and 68.92 ± 0.9 MPa, respectively. Also, the manufactured samples made of PA6 under the liquefier temperature of 220 °C had the lowest strength. Indeed, the weak adhesion between the deposited layers in the manufactured samples made of PA6 under the liquefier temperature of 220 °C, did not let

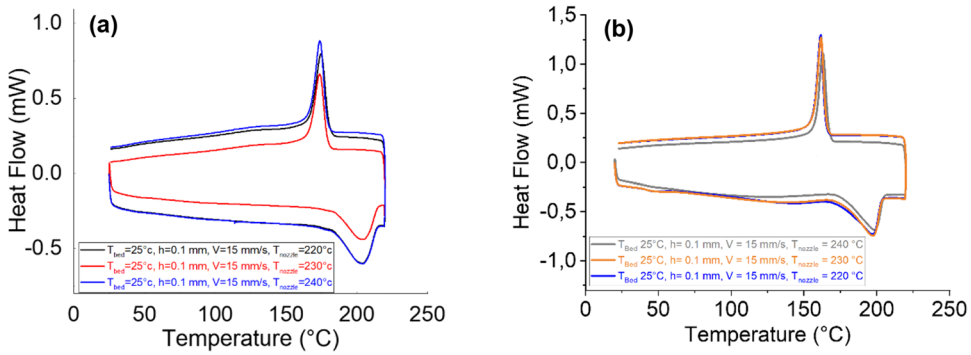

Fig. 7 DSC results for fabricated samples PA6 (**a**) and CF-PA6 (**b**) [31] under the different liquefier temperatures

Table 2 The obtained values related to different properties from DSC curves concerning the printed PA6 and CF-PA6 samples

Conditions		T_c (°C)	T_m (°°C)	%Crystallinity
PA6	$T_{Liquefier}$ = 220 °C	174.83 °C	204.51 °C	12.51%
	$T_{Liquefier}$ = 230 °C	173.73 °C	207.74 °C	12.75%
	$T_{Liquefier}$ = 240 °C	174.02 °C	207.82 °C	14.40%
CF-PA6	$T_{Liquefier}$ = 220 °C	161.5 °C	197.5 °C	19.97%
	$T_{Liquefier}$ = 230 °C	161.7 °C	197.7 °C	20.26%
	$T_{Liquefier}$ = 240 °C	162.8 °C	198.7 °C	20.51%

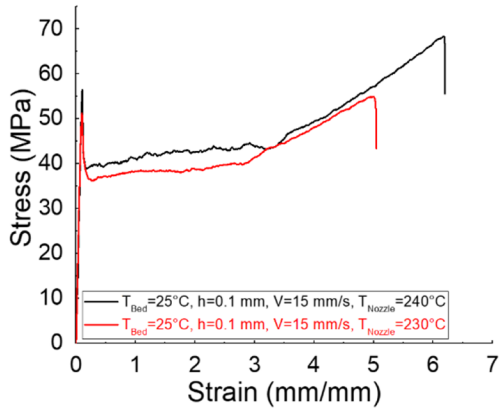

Fig. 8 Tensile behavior of the printed PA6 specimens under the various liquefier temperatures

us even to cut the printed single-wall samples (Fig. 1b) to prepare the required tensile test specimen (Fig. 3). Because the undesirable fracture occurred in the interface of the deposited layers during the cutting/punching process. Also, the crystallinity percentage of the manufactured PA6 samples under 220, 230, and 240 °C were 12.51%, 12.75%, and 14.40%, respectively. So, as it was found out from the obtained results, by increase of the liquefier temperature, the crystallinity percentage was increased, too. Moreover, this increasing trend was observed in the obtained tensile strength.

While according to the recent conducted research concerning the CF-PA6 samples, the obtained tensile strength under the liquefier temperature values of 220, 230, and 240 °C were 49 ± 1.5, 51 ± 3, and 55 ± 0.6 MPa, respectively. Also, the obtained crystallinity percentage of the related manufactured CF-PA6 samples under 220, 230, and 240 °C were 19.97%, 20.26%, and 20.51%, respectively.

As it was observed, the crystallinity percentage values of the manufactured CF-PA6 samples were more than the correlated PA6 manufactured samples. In fact, the existed chopped carbon fibers in CF-PA6 had been the preferable crystalline nucleation sites. Also, the strength of the CF-PA6 samples obtained from the printed single-wall parts had lower strength in comparison with the ones made of PA6. It can be due to the rotation and sort of turbulent movement of chopped carbon fibers among the printing process and avoid of the suitable polymer/matrix fluidity between the fibers while the matrix had been in the liquid and even semi solid state. Which caused narrow sections in some sections of solidified raster (Fig. 9). The narrow sections appeared because of the lack of enough fluidity of matrix and increase of the viscosity due to the existence of the chopped carbon fibers. These sections (determined in Fig. 9) were stress concentration locations, which caused less strength of the prepared CF-PA6 samples from the printed single-wall parts comparing PA6 samples.

4.2.2 Influence of print speed

The impact of the print speed as another important additive manufacturing process parameter of the manufactured samples made of CF-PA6 and PA6 was investigated, too. This parameter has an effective and direct correlation with the production consumed time and consequently the production expenditures. For this aim, three different values of 13, 15, and 17 mm/s were selected to manufacture the related specimens. The crystallinity percentage of the corresponded samples were calculated from the obtained results from DSC characterization. The obtained crystallinity percentage values are tabulated in Table 3. This table depicts the effect of

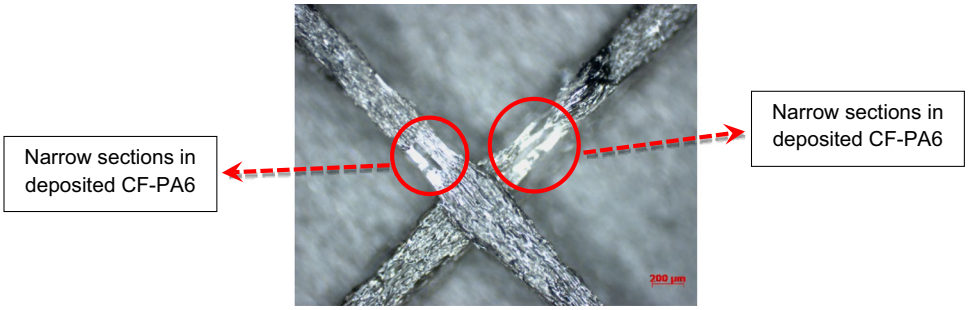

Fig. 9 Observed narrow sections in the deposited CF-PA6 raster [5]

Table 3 The obtained values related to different properties from DSC curves concerning the printed PA6 and CF-PA6 samples at the different print speeds

Conditions		T_c (°C)	T_m (°C)	%Crystallinity
PA6	V = 13 mm/s	169.98 °C	206.80 °C	15.46%
	V = 15 mm/s	174.02 °C	207.82 °C	14.44%
	V = 17 mm/s	170.17 °C	206.71 °C	15.67%
CF-PA6	V = 13 mm/s	161.68 °C	197.71 °C	20.77%
	V = 15 mm/s	162.82 °C	198.72 °C	20.51%
	V = 17 mm/s	161.94 °C	197.60 °C	20.64%

the considered print speed values on T_m, T_c, and the crystallinity percentage of the FFF-processed PA6 and CF-PA6 specimens. No highlighted thermal effect due to the selected print speed values on the utilized PA6 and CF-PA6 materials were observed.

The obtained tensile strength of the CF-PA6 specimens manufactured by the print speeds of 13, 15, and 17 mm/s were 65 ± 0.5, 55 ± 0.6, and 63 ± 1.3 MPa, respectively. Also, according to the applied tensile tests on the PA6 printed specimens at the stated different print speed values, the tensile strength values of 57.78 ± 0.84, 68.92 ± 0.9, and 69 ± 0.05 MPa were obtained related to the printed specimens at the print speed of 13, 15, and 17 mm/s, respectively (Fig. 10). Thus, as the general observation, it was understood that by increase of the print speed of the manufacturing process of the PA6 specimens, the related strength of the specimens was increased, too. Moreover, the obtained tensile strength of the manufactured PA6 samples with the print speed values of 15 and 17 mm/s were more than the manufactured CF-PA6 specimens with the same print speed values. It can be due to the rotation and sort of turbulent movement of the chopped carbon fibers and consequent inappropriate fluidity of the matrix polymer during the deposition process.

To analyze this phenomenon, in-situ temperature measurements of the manufactured CF-PA6 samples by the different print speeds of 13, 15, and 17 mm/s are presented in Fig. 11. The results exhibit that by an increase of the printing speed, the temperature evolution of the first printed

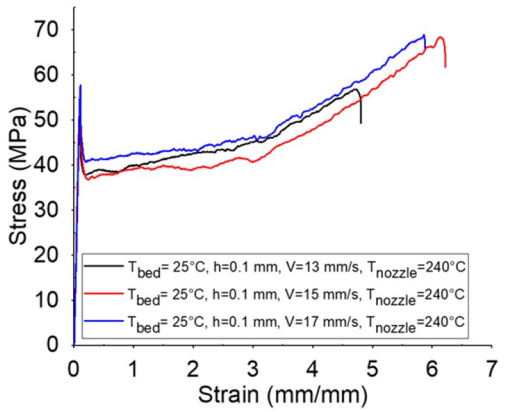

Fig. 10 Tensile behavior of FFF-processed PA6 specimens under the various print speed values

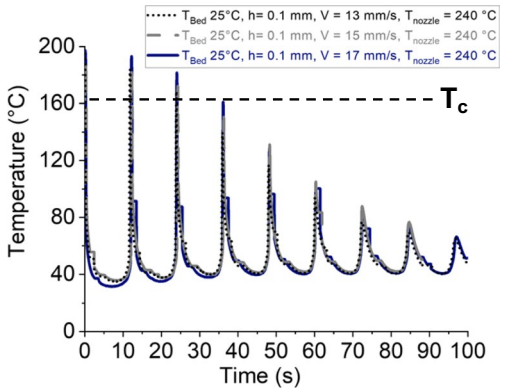

Fig. 11 In situ temperature measurement obtained for different print speeds (CF-PA6) [31]

layer remains above the crystallization temperature in the printed specimens with the three considered printing speed values. The same was observed in the obtained curve from in situ temperature measurements of the manufactured PA6 parts (Fig. 12). Due to the increased print speed, the polymer chains are rearranged and the degree of crystallinity is subsequently higher as a result of the shorter cooling time. This could contribute to poor dimensional stability.

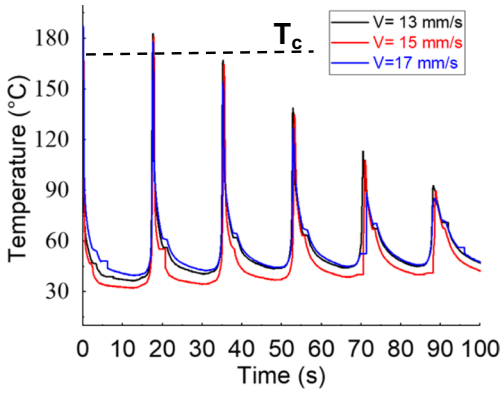

Fig. 12 In situ temperature measurement for different print speed (PA6) [5]

According to Fig. 13, the obtained time–temperature curve related to the printed samples made of PA6 and CF-PA6 under the print speed of 15 mm/s had the same evolution. This evolution can confirm that the presence of the chopped carbon fibers has no significant effect on the temperature evolution of the filament in the printing process under the condition of the selected print speed values. So, the observed different trends in the tensile strength values of PA6 and CF-PA6 specimens was due to the existence of the short carbon fibers (reinforcement component of the composite material). The short carbon fibers could not influence the temperature evolution of the deposited layers during the manufacturing process of the specimens, significantly. The chopped carbon fibers could just effect on the fluidity of the polymer (the matrix component of the composite material), which has discussed in the conducted study about the liquefier temperature effect.

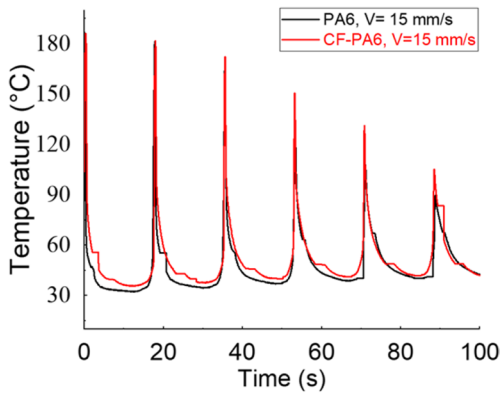

Fig. 13 In situ temperature measurement of manufactured PA6 and CF-PA6 samples at the print speed 15 mm/s

4.2.3 Influence of layer height

The study has been conducted on the effect of the layer height as a process parameter in the fused filament fabrication (FFF) of CF-PA6 [31] and PA6 [5]. For the purpose of studying the impact of this process parameter on the mechanical behavior of the obtained specimens, three different layer height values of 0.1, 0.2, and 0.3 mm were utilized in the printing process. As the obtained result from the tensile test concerning the composite (CF-PA6) samples, the printed specimens with the selected layer height values of 0.1, 0.2, and 0.3 mm had respective tensile strengths of 55 ± 0.6, 49 ± 2.5, and 56 ± 2.5 MPa. For the better understanding of the effect of this process parameter, the in situ temperature measurement was carried out during the manufacturing process of CF-PA6 samples with the stated different layer height values. It was proposed that there were two diverse factors influencing the mechanical behavior of the manufactured samples by FFF with the stated different layer height values. Which were (i) decrease of the liquidity (or fluidity) of the printed layers, and (ii) increase of the retained temperature in the printed layers. It was proposed that the second competition factor was overridden in the CF-PA6 manufacturing process by shifting the layer height from 0.1 to 0.2 mm due to a proposed decrease in liquidity (or fluidity). It was concluded that the fluidity had decreased based on the peaks which were observed in the temperature evolution (time–temperature) curves, where the maximum temperature of each printed layer with 0.1 mm of layer height was greater than the maximum temperature of the deposited layer with 0.2 mm of layer height (Fig. 14). Figure 14 depicts the peaks of the first-four consecutive CF-PA6 layers with the height of 0.1 and 0.2 mm. It is derived from the time–temperature curve observed during in situ measurement. This resulted in a decrease in the adhesion and the bonding of the printed layers and the subsequent reduction

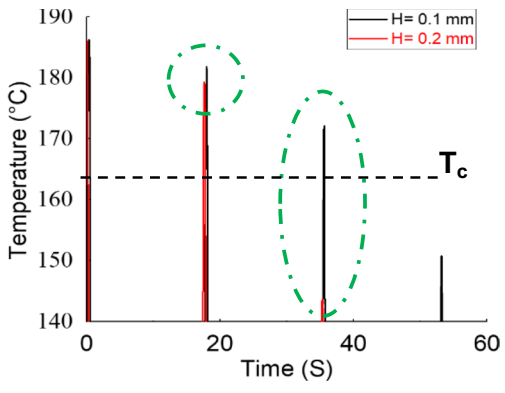

Fig. 14 Peaks of the first-four CF-PA6 deposit layers with the height of 0.1 mm and 0.2 mm obtained from the conducted in situ temperature measurement [5]

in the strength of the printed samples with the layer heights of 0.2 mm comparing to 0.1 mm samples.

For the better understanding the observed phenomenon in the trend of the tensile strength values by increase of the layer height from 0.1 to 0.2 mm, some samples made of PA6 (without any utilized reinforcement components) were manufactured. The manufactured samples were printed with the layer height of 0.1 and 0.2 mm. In the case of the manufactured PA6 samples with the layer heights of 0.1 mm and 0.2 mm, the obtained tensile strength values were 68.92 ± 0.9 and 72.57 ± 0.8 MPa, respectively. So, by considering the increase in the strength of the manufactured PA6 samples by increase of layer height from 0.1 to 0.2 mm, it was found out that the decrease of the liquidity (or fluidity) factor wasn't sensible in case of the PA6 samples. It is worthy of note that the decreased liquidity factor (or fluidity factor) could also be a result of chopped carbon fibers. Indeed, the chopped carbon reinforcements were the solid components in the liquid/semi-liquid polymer matrix component of the composite material during the FFF process. Therefore, the solid chopped carbon fibers caused the fluidity decrease of the matrix component during the FFF process.

Although in the case of the FFF process of CF-PA6, with the layer height 0.3 mm, it is suggested that an increase in the retained temperature in the printed layers has overcome the first competitive factor. However, as can be observed in the bottom of the time–temperature curve (lower limit) concerning the printed samples with the layer height of 0.3 mm (Fig. 15), more temperature value causes chain rearrangement and consequently an increase in crystallinity percentage with modification of the mechanical behavior. So, the obtained crystallinity percentage of the manufactured CF-PA6 samples with the layer heights of 0.1 and 0.3 mm were 20.51% and 21.22%, respectively.

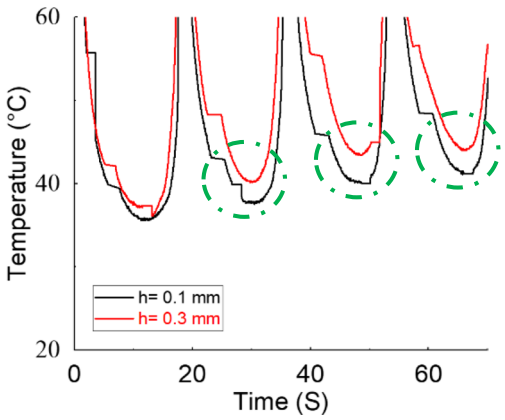

Fig. 15 Lower limit of temperature profile of the fourth CF-PA6 deposit layers with height of 0.1 mm and 0.3 mm obtained from the performed In-situ temperature measurement [5]

4.2.4 Influence of bed temperature

As a part of the evaluation of the bed temperature effect on the FFF processed samples, the dimensional stability of the manufactured samples were evaluated. The bed temperature is the bed platform temperature. Indeed, it is concerning the temperature of the plateau where the extruded layers will be deposited there and consequently, the specimens will be formed layer-by-layer there. Four different bed temperatures of 25, 50, 60, and 80 °C were considered to print the related samples. So, the dimensional accuracy of the deposited layers in the manufactured samples made of PA6 were evaluated. Indeed, the bed platform temperatures were selected based on their differences from T_g of the utilized PA6 filament (45 °C). Accordingly, the temperature values of 25, 50, 60, and 80 °C were considered. Indeed, the 20 °C temperature selected for bed platform is below T_g, while the other selected temperatures (50, 60, and 80 °C) exceed Tg to a varying extent. According to the optical microscopy (OM) observations (Fig. 16), the irregularity in the deposition pattern and consequent poor dimensional accuracy were observed in the deposited layers of the FFF processed samples which were manufactured at the bed temperature value of 80 °C (the highest selected bed temperature value) comparing to the printed sample at the bed temperature value of 25 °C (the lowest selected bed temperature value).

Moreover, the stated dimensional accuracy decrease by the bed temperature increase had been observed in the manufactured samples made of CF-PA6 [31]. Figure 17 depicts the temperature measurements made in situ of the manufacturing process for the FFF processed PA6 specimens with the miscellaneous selected bed temperature values. Moreover, according to Fig. 17, the lower limits of the Time–Temperature curves were increased by the increase of the bed platform temperature. Almost all printed specimens reached near crystallization temperatures after the first layer deposition by applying the bed temperatures outlined above. However, the dimensional instability issue was more pronounced with the FFF processed specimens at the bed temperature of 80 °C. So, the same trend in dimensional accuracy was observed in the case of the CF-PA6 and PA6 specimens, Thus, the chopped carbon fibers could not cause any modifications on the decrease of the dimensional accuracy by the bed temperature increment.

4.3 Analyses of the microstructures of the FFF processed specimens

The widths of the ten consecutive deposited layers were measured in order to evaluate the microstructure of the manufactured PA6 specimens. A representative example of this

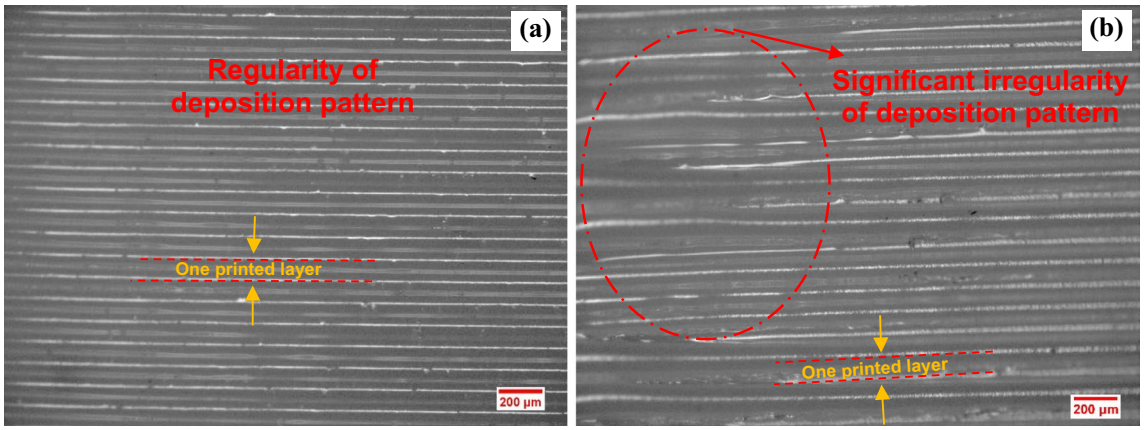

Fig. 16 OM micrographs related to the PA6 printed specimens at the bed temperature values of 25 °C (**a**) and 80 °C (**b**) [5]

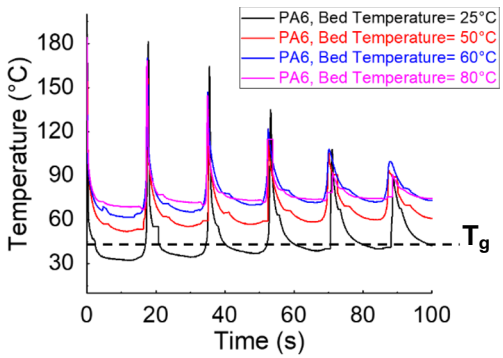

Fig. 17 Thermal measurements of the printed specimens with the different bed temperatures [5]

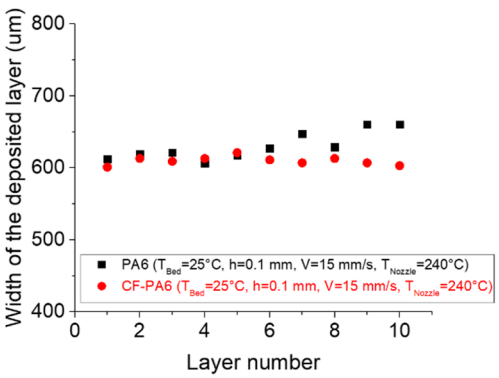

Fig. 19 Comparing the width size of the deposited layers in the PA6 and CF-PA6 specimens manufactured under the same process parameters condition

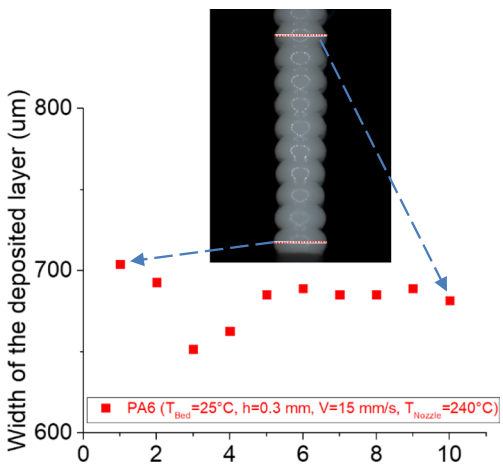

Fig. 18 Analysis of the width of the deposited layers in the PA6 specimen

analysis can be found in Fig. 18, which depicts the FFF processed PA6 sample at the bed temperature, layer height, print speed, and nozzle temperature respective to 25 °C, 0.3 mm, 15 mm/s, and 240 °C. In fact, the unity of the width of the deposited layers will result in suitable dimensional stability of the manufactured parts/specimens.

By the extension of this study on the large quantity of the consecutive layers, a decrease in the width size of the deposited layer was observed, generally. Due to the stated temperature evolution of the deposited layers, it can be observed that the temperature fell below the crystallization temperature after two or three sequences of the deposition. As the result, it increases the cooling rate, solidifies the material, reduces material diffusion, reduces the width of deposited layers, and ultimately reduces the contact surface between the two adjacent deposited layers.

The final features and microstructure of the parts were influenced by each type of the selected printing process condition. According to the aforementioned observations, the same evaluation was applied on the deposit layers (Fig. 19) to evaluate the width size of the deposited layers in the FFF-processed PA6 and CF-PA6 under the determined reference

manufacturing condition for the CF-PA6 samples [31]. The reference condition of the processing parameters was the layer height, bed temperature, liquefier temperature, and print speed of 0.1 mm, 25 °C, 240 °C, and 15 mm/s, respectively. In light of the foregoing observations, the same evaluation was applied on the deposited layers in the PA6 and CF-PA6 manufactured samples fabricated under the determined FFF processing reference conditions for the CF-PA6 sample. Afterward, the width sizes of the deposited layers were compared to understand how the carbon fiber reinforcements affected the dimensional accuracy and stability of the FFF processed specimens.

According to Fig. 19, the unity of the width size in the CF-PA6 samples were more obvious comparing to PA6 specimens. In such a way that the obtained curve concerning CF-PA6 exhibit an almost linear regime. As a matter of fact, during the FFF process, the chopped carbon fibers could control the fluctuations of the width size of the deposited layers and could result in suitable dimensional accuracy/stability in the manufactured CF-PA6 specimens. Also, according to D. Stoof et al. [37] As fiber content increased in PP, shrinkage decreased across all manufactured composites.

4.4 Thermal properties and rheological analysis: time–temperature-transformation diagram

During the FFF process, the thermal properties, and the rheological properties of the utilized polymers (also the matrix of the polymer-based composite) have the essential and significant role. The adhesion of the deposited layers in the final manufactured part is depended on this role. A part of the presented study is concerned with the temperature and its effect on the viscosity of the polymer and the matrix component of the composite material (CF-PA6) (Fig. 20).

As was stated in FFF process, a thermoplastic polymer is fed into a liquefier that extrudes a filament while moving in successive X–Y planes along the Z direction, to fabricate a 3D part layer-by-layer. Consequently, as the deposition progresses, the hot filament is deposited onto filaments that were previously deposited and also are situated in the cooling process. This causes their re-heating, defining a time when the interfaces of contacting filaments are above the glass transition temperature (T_g) in the case of amorphous materials, or of the crystallization temperature (T_c) for semi-crystalline materials, which is necessary for proper bonding occurrence. Therefore, each filament should be sufficiently hot during deposition, but not too hot, to avert deformation due to gravity and to the weight of the filaments deposited in subsequent layers.

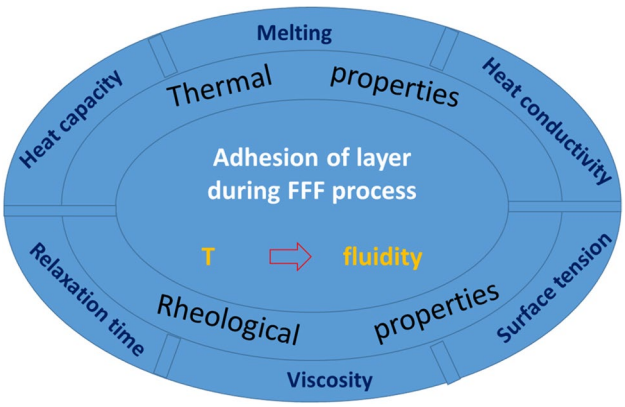

Fig. 20 General view of the FDM process of polymer and composite materials and the obtained adhesion of the deposited layers

In the previous conducted study, it was turned out that the optimal condition of the selected process parameters for FFF processing of the CF-PA6 samples were; liquefier temperature: 240 °C, print speed: 15 mm/s, layer height: 0.1 mm, and platform temperature: 25 °C. Time–temperature-transformation diagram concerning the optimal condition of CF-PA6 was plotted. The provision of this curve help designers to consider the processability condition of the applied material. Which help the manufacturer to optimize the manufacturing parameters of FFF processes in order to maximize the mechanical performance and the dimensional stability of the parts.

Regardless of the study on the influence of the process parameters on the neck-growth prediction by viscoelastic models, there is still a lack of practical knowledge on consideration of temperature dependent viscosity and its influence on coalescence of the two adjacent filaments. To eliminate the mentioned missing spot, a thermo-mechanical approach is an essential manner by applying the results of temperature evolution of filaments at their interface.

The evolution of viscosity as a function of time and temperature by the following two methods have been determined:

- *By rheometer*; in the molten state (the used temperature for studying the effect of the liquefier temperature 210, 220, 230, and 240 °C)
- *By DMTA*; in the rubbery state (between T_c and T_g)

Rheometry tests were performed at varying shear rates in isotherm regime. Several tests were carried out at the different temperatures. Using DMTA, multi-frequency testing from 1 to 30 Hz was performed.

4.4.1 Viscosity measurement at molten state

The temperature evolution during the cooling stage (and thus the re-heating peaks) of a deposited filament plays an important role in the determination of the filament bonding through deposition. Also, the correlation of rheological

characteristic along with the mechanical properties is a key point. So, simultaneous characterization of the thermal and rheological properties is inevitable. Regarding the mechanism of deposition and temperature profile of each layer, viscosity varies accordingly. In general, following observations could be concluded:

- Lower cooling rate limits the viscosity enhancement.
- By cooling of the deposited filament from a temperature of the extruder to the ambient temperature, the viscosity varies depending on the deposition conditions.
- Viscosity tends to unlimited values depending on the filament's temperature evolution.

One benefit of temperature dependence viscosity consideration over the FFF process is that it enables us to have more precise investigations of rheological characteristics. This issue could be more highlighted while considering the interaction of engaged parameters through them. This is a potential concern by which engaged researchers in the study of the bonding and mechanical strength.

The evolution of viscosity and temperature were considered, simultaneously. The temperature dependence viscosity was considered to vary from the liquefier temperature to the ambient temperature using the Arrhenius equation by implementing the temperature evolution. The obtained curves from viscosity measurements of PA6 and CF-PA6 are presented in Fig. 21.

The viscosity variation in the melt state as a function of temperature obeys Arrhenius law (Eq. 1). As for showing the validity of this law for the PA6 and CF-PA6 in the molten state, we determined the Newtonian viscosity of the stated materials at the different temperatures by performing isothermal tests. According to this equation, by plotting $\ln\eta$ as the function of $^1/_T$, we will obtain the following equation that is a linear function:

$$\ln\eta = \ln\eta_0 + \left(\frac{E}{R}\right) \times \frac{1}{T} \tag{1}$$

Figure 22 clearly demonstrates the measured value for viscosity at the different temperature and isotherm state, related to PA6 and CF-PA6. The values could be fit to the mentioned equation and the related curve, which means that the constants of this law—E and η_0—for PA6 are 30.36 kJ and 4.93 Pa.s, respectively. Also, the constants of this law—E and η_0—for CF-PA6 are 42.93 kJ and 0.5 Pa.s, respectively.

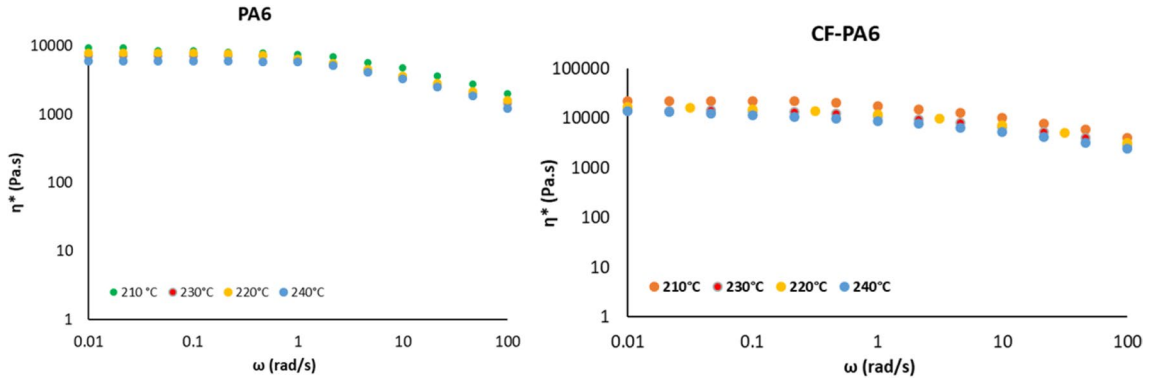

Fig. 21 Viscosity evolution in the different temperature values related to PA6 (left) and CF-PA6 (right)

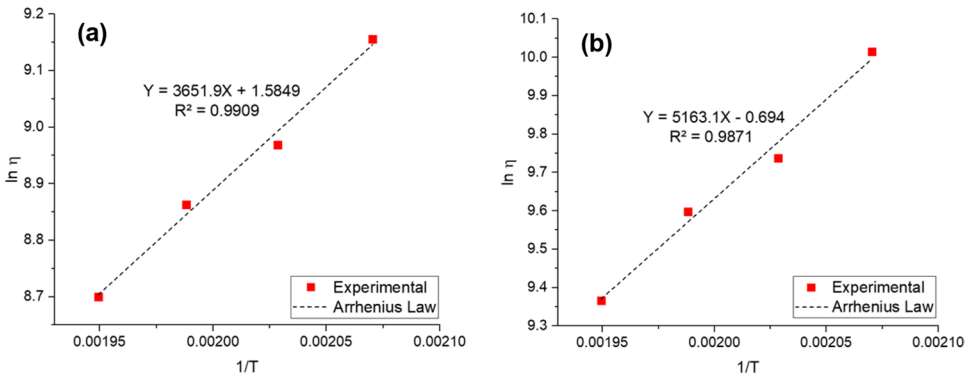

Fig. 22 Ln (η) versus 1/T related to **a** PA6 and **b** CF-PA6

4.4.2 Viscosity measurement at solid state

Consequently, to explore the influence of temperature on viscoelastic properties of PA6 and CF-PA6, multi-frequencies DMA test was implemented in the flexural bending mode. The obtained curves related to CF-PA6 are presented in Fig. 23.

The evolution of viscosity could be calculate using Williams-Landel-Ferry (WLF) equation:

$$Loga_T = \frac{-C_1(T - T_r)}{C_2 + (T - T_r)} \tag{2}$$

where a_T is WLF shift factor, C_1 and C_2 are empirical constants adjusted to fit the values of superposition parameter a_T, T is the temperature, and T_r is the reference temperature at reference frequency.

Using linear regression method, WLF equation could be transformed to the following equation:

$$\frac{1}{Loga_T} = \frac{-C_2}{C_1}\frac{1}{T - T_r} + \frac{1}{C_1} \tag{3}$$

Then, $\frac{1}{Loga_T}$ was plotted versus $\frac{1}{T-T_r}$. The fitted curves are shown in Fig. 24 ($R^2 = 0.9869$ related to PA6 and $R^2 = 0.9993$ related to CF-PA6). The value of C_1 and C_2 are then calculated using the obtained results.

4.4.3 Time–temperature-transformation diagram

The main characteristic of the presented approach is the possibility of the obtaining a time–temperature-transformation diagram of the applied material which is related to the features of the material during deposition process. It will let us apply the obtained results to have an optimized manufacturing process. It has been shown that the affected viscosity by the cyclic temperature profile exists in FFF process could determine the characteristic of final products. Its variation through the consequence of layers has been presented. Furthermore, a parametric study on the influence of process parameters upon viscosity evolution has also been performed. The influence of print speed and platform temperature on the evolution of viscosity indicate that the effect of process parameters is inevitable, and interaction of parameters should be taken into account.

A zoom of the processability areas of PA6 and CF-PA6 in FFF show that the zone of processability is approximately between 240 and 162 °C (CF-PA6)/173 °C (PA6)

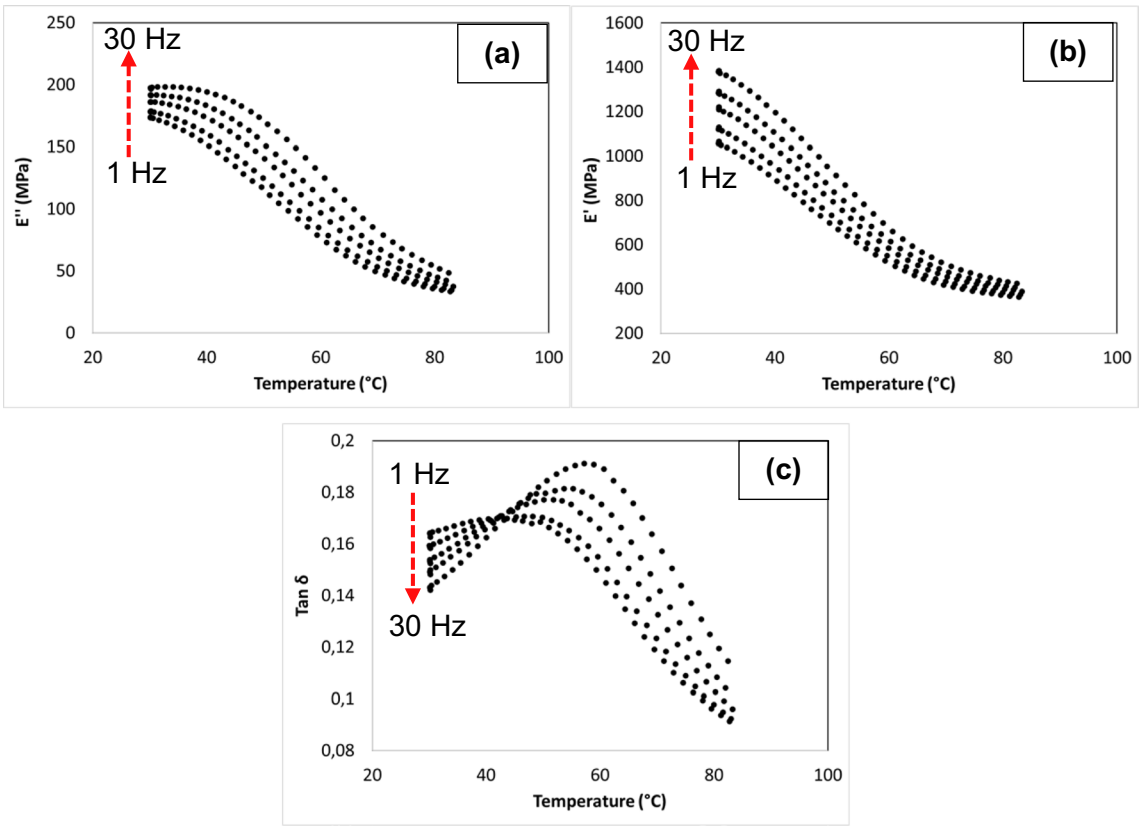

Fig. 23 DMTA test result: evolution of the **a** loss moduli, **b** storage moduli, and **c** loss factor versus temperature for CF-PA6

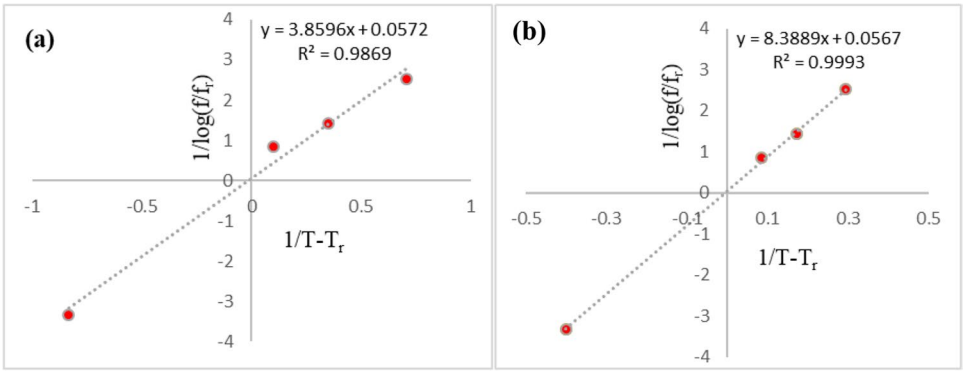

Fig. 24 Linear regression of WLF equation related to **a** PA6 and **b** CF-PA6

while cooling down. And during this cooling stage, viscosity raised suddenly from 650 to 104 Pa.s (Fig. 25).

As a result, the variation in viscosity as a function of temperature can be modeled over a wide temperature range. Also, the influence of cyclic temperature profile on viscoelastic behavior of the material using WLF equation indicated that the viscosity variation in the solid state plays an important role on the rheological characteristic of the material. The presented results may help researchers and manufacturer to improve the quality of constructed parts by FFF and consequently ameliorate their strength. Understanding the processability area allows us to optimize the FFF process more easily.

5 Conclusions and outlook

This paper prepared an investigation concerning the influence of some important FFF process parameters on the rheological properties of CF-PA6 and PA6 during the FFF process and the subsequent effects on the inter-layer adhesion (bonding) of the deposited layers. Therefore, the effect of chopped carbon fibers on the modification of the rheological properties of the parts during and after FFF process was investigated. This study helped the researchers and manufacturers to understand better the impact of the chopped carbon fibers as the reinforcement on the rheological and mechanical properties of the FFF-processed CF-PA6 parts. The physicochemical, thermal and mechanical characterizations revealed the impact of the chopped carbon fibers on the cooling stage of the deposited polymer layers (matrix component) and subsequently the crystallinity percentage. The crystallinity percentage can affect the diffusion of the polymer material during the FFF process and consequently affect the mechanical performance and the dimensional stability of the manufactured parts. It was turned out that the performance of the FFF-processed parts can be altered or modified under the specific selected process parameters by the chopped carbon fiber reinforcement. The FFF-processed PA6 and chopped carbon fiber reinforced PA6 materials perform differently during FFF process under the same selected process parameters. Finally, a time–temperature-transformation (TTT) diagram can be generated by examining the effect of the selected process parameters on the materials during and after the FFF process. This curve can determine the processability condition of our materials. It

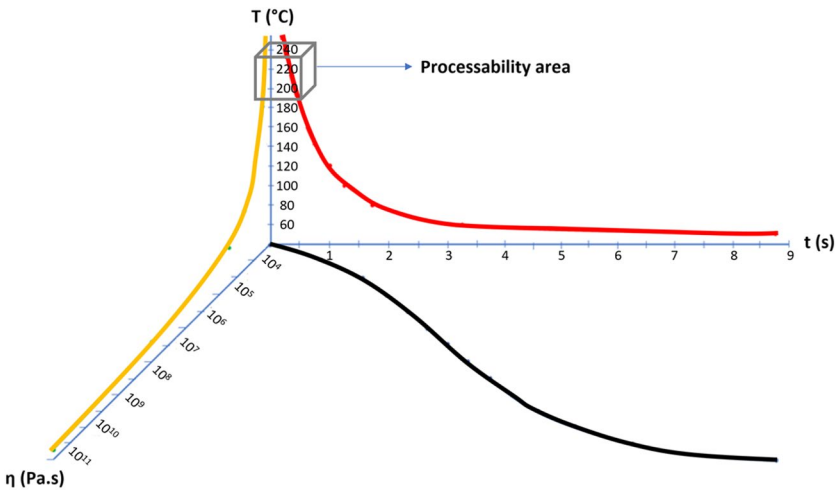

Fig. 25 Time–temperature-transformation diagram: PA6 and CF-PA6

can be helpful for the designers and researchers to find out the optimal FFF process parameter conditions for a specific utilized raw material.

Declarations

Ethics approval All the authors declare that this paper did not need ethics approval.

Consent to participate Not applicable.

Consent for publication Not applicable.

Conflict of interest The authors declare no competing interests.

References

1. Standard, A. S. T. M. (2012) F2792. 2012 Standard terminology for additive manufacturing technologies. ASTM International, West Conshohocken. See www.astm.org. https://doi.org/10.1520/F2792-12
2. Ahmadifar Mohammad et al (2021) Additive manufacturing of polymer-based composites using fused filament fabrication (FFF): a review. Appl Compos Mater 28:1335–1380
3. Górski FILIP, Kuczko WIES, Wichniarek RADOSŁAW (2014) Impact strength of ABS parts manufactured using fused deposition modeling technology. Arch Mech Technol Autom 34(1):3–12
4. Baich L, Manogharan G, Marie H (2015) Study of infill print design on production cost-time of 3D printed ABS parts. Int J Rapid Manuf 5(3–4):308–319
5. Ahmadifar M, Benfriha K, Shirinbayan M (2023) Thermal, tensile and fatigue behaviors of the PA6, short carbon fiber-reinforced PA6, and continuous glass fiber-reinforced PA6 materials in fused filament fabrication (FFF). Polymers 15(3):507
6. Ahn Daekeon et al (2012) Quantification of surface roughness of parts processed by laminated object manufacturing. J Mater Proc Technol 212(2):339–346
7. Wang Jie et al (2016) Stereolithographic (SLA) 3D printing of oral modified-release dosage forms. Int J Pharm 503(1–2):207–212
8. Greiner Sandra et al (2017) Selective laser sintering of polymer blends: bulk properties and process behavior. Polymer Test 64:136–144
9. Turner BN, Strong R, Gold SA (2014) A review of melt extrusion additive manufacturing processes: I Process design and modeling. Rapid Prototyp J 20(3):192–204
10 Yeole P et al (2020) Mechanical characterization of high-temperature carbon fiber-polyphenylene sulfide composites for large area extrusion deposition additive manufacturing. Addit Manuf 34:101255
11. Ning F et al (2017) Additive manufacturing of carbon fiber-reinforced plastic composites using fused deposition modeling: effects of process parameters on tensile properties. J Compos Mater 51(4):451–462
12. Wong KV, Hernandez A (2012) A review of additive manufacturing. ISRN Mech Eng 2012:1–10
13. Li N, Li Y, Liu S (2016) Rapid prototyping of continuous carbon fiber reinforced polylactic acid composites by 3D printing. J Mater Process Technol 238:218–225
14 Zhang J et al (2019) Molding process and properties of continuous carbon fiber three-dimensional printing. Adv Mech Eng 11(3):1687814019835698
15. Tian X et al (2016) Interface and performance of 3D printed continuous carbon fiber reinforced PLA composites. Compos Part A Appl Sci Manuf 88:198–205
16. Mori K-I, Maeno T, Nakagawa Y (2014) Dieless forming of carbon fibre reinforced plastic parts using 3D printer. Procedia Eng 81:1595–1600
17. Nakagawa Y, Mori K-I, Maeno T (2017) 3D printing of carbon fibre-reinforced plastic parts. Int J Adv Manuf Technol 91(5):2811–2817
18. Namiki M, Ueda M, Todoroki A, Hirano Y, Matsuzaki R (2014) 3D printing of continuous fiber reinforced plastic. In: SAMPE Tech Seattle 2014 Conference. Soc. for the Advancement of Material and Process Engineering
19 Wu S et al (2019) 3D-printed chiral metasurface as a dichroic dual-band polarization converter. Optics Lett 44(4):1056–1059
20. Wang X, Jiang M, Zhou Z, Gou J, Hui D (2017) 3D printing of polymer matrix composites: a review and prospective. Compos Part B Eng 110:442–458
21. Too MH et al (2002) Investigation of 3D non-random porous structures by fused deposition modelling. Int J Adv Manuf Technol 19(3):217–223
22. Masood SH, Rattanawong W, Iovenitti P (2000) Part build orientations based on volumetric error in fused deposition modelling. Int J Adv Manuf Technol 16(3):162–168
23. Zander NE, Gillan M, Lambeth RH (2018) Recycled polyethylene terephthalate as a new FFF feedstock material. Addit Manuf 21:174–182
24. Chong S et al (2017) Physical characterization and pre-assessment of recycled high-density polyethylene as 3D printing material. J Polym Environ 25(2):136–145
25. Pakkanen J, Manfredi D, Minetola P, Iuliano L (2017) About the use of recycled or biodegradable filaments for sustainability of 3D printing. State of the art and research opportunities. Sustainable Design and Manufacturing 2017: Selected papers on Sustainable Design and Manufacturing 4:776–785
26 Tekinalp HL et al (2014) Highly oriented carbon fiber–polymer composites via additive manufacturing. Compos Sci Technol 105:144–150
27. Fu S-Y et al (2000) Tensile properties of short-glass-fiber-and short-carbon-fiber-reinforced polypropylene composites. Compos A Appl Sci Manuf 31(10):1117–1125
28. Fu S-Y, Lauke B (1996) Effects of fiber length and fiber orientation distributions on the tensile strength of short-fiber-reinforced polymers. Compos Sci Technol 56(10):1179–1190
29. Costa AE, da Ferreira Silva A, Sousa Carneiro O (2019) A study on extruded filament bonding in fused filament fabrication. Rapid Prototyp J 25(3):555–565
30. Shofner ML et al (2003) Nanofiber-reinforced polymers prepared by fused deposition modeling. J Appl Polym Sci 89(11):3081–3090
31. Benfriha K, Ahmadifar M, Shirinbayan M, Tcharkhtchi A (2021) Effect of process parameters on thermal and mechanical properties of polymer-based composites using fused filament fabrication. Polym Compos 42(11):6025–6037
32 Brenken B et al (2019) Development and validation of extrusion deposition additive manufacturing process simulations. Addit Manuf 25:218–226
33. Gupta A et al (2020) Processing, mechanical characterization, and micrography of 3D-printed short carbon fiber reinforced polycarbonate polymer matrix composite material. Int J Adv Manuf Technol 107(7):3185–3205

34. Choi Y-H et al (2016) Influence of bed temperature on heat shrinkage shape error in FDM additive manufacturing of the ABS-engineering plastic. World J Eng Technol 4(3):186–192
35. Ning F et al (2015) Additive manufacturing of carbon fiber reinforced thermoplastic composites using fused deposition modeling. Compos Part B Eng 80:369–378
36. Zhong W et al (2001) Short fiber reinforced composites for fused deposition modeling. Mater Sci Eng A 301(2):125–130
37. Stoof D, Pickering K (2018) Sustainable composite fused deposition modelling filament using recycled pre-consumer polypropylene. Compos B Eng 135:110–118